

Research Article

Adsorption of Water Molecule in Graphene/MoS₂ Heterostructure with Vacancy Defects in Mo Sites

Hari Krishna Neupane ^{1,2} and Narayan Prasad Adhikari ²

¹Amrit Campus, Institute of Science and Technology, Tribhuvan University, Kathmandu, Nepal

²Central Department of Physics, Institute of Science and Technology, Tribhuvan University, Kathmandu, Nepal

Correspondence should be addressed to Narayan Prasad Adhikari; npadhikari@gmail.com

Received 22 December 2021; Revised 25 February 2022; Accepted 3 March 2022; Published 11 April 2022

Academic Editor: Sefer Bora Lisesivdin

Copyright © 2022 Hari Krishna Neupane and Narayan Prasad Adhikari. This is an open access article distributed under the Creative Commons Attribution License, which permits unrestricted use, distribution, and reproduction in any medium, provided the original work is properly cited.

First-principle calculations based on the spin-polarized density functional theory (DFT) with vdW corrections by DFT-D2 approach have been carried out to study structural, electronic, and magnetic properties of water-adsorbed graphene/MoS₂ heterostructures (system-I), and water-adsorbed graphene/MoS₂ heterostructures with vacancy defects in Mo sites (systems-II). We consider vacancy defects in different Mo sites such as centre-1Mo atom vacancy defect (system-IIa), left-1Mo atom vacancy defect (system-IIb), and 2Mo atom vacancy defects (system-IIc). All the systems considered in this study are structurally stable; however, the stability of defected systems decreases with an increase in defect concentrations. The calculated binding energies of HS used in this study agree with the reported work. Electronic properties of system-I and systems-II reveal that they have metallic characteristics. Our investigation shows that system-I is nonmagnetic and systems-II are magnetic. The magnetic moment in the defected systems (system-IIa, system-IIb, and system-IIc) is developed by unpaired up and down-spins of electrons created in the orbitals of atoms due to vacancy defects in Mo atoms.

1. Introduction

One of the ways to create 2D heterostructures is by two or more monolayers of different materials. The heterostructures improve the functional characteristics and bear novel properties. Therefore, they have intrigued the advanced compliance of researchers to predict other advantageous properties than the constituents [1, 2]. Presently, two-dimensional (2D) van der Waals (vdW) graphene/MoS₂ (G/MoS₂) heterostructure (HS) is a useful tool to design applicable electronic devices [3–6]. Graphene is an atom-thick 2D honeycomb lattice, and has a series of special electronic and physical properties. Its exceptional physical strength, large surface area, high electrical and thermal conductivities, low noise effect, controllable tunable band structure, and many more other interesting properties explore multiple possible applications such as electronic, spintronics, and gas sensors [1, 7–10]. 2D Molybdenum disulphide (MoS₂) is the form of hexagonal plane crystal

structure of S atoms on either side of a hexagonal plane of Mo atoms. It has certain bandgap in its electronic band known as the wide bandgap exotic semiconductor [11, 12]. MoS₂ is used in the electronic, spintronic, and optoelectronic devices because of its impressive optical, electronic, and magnetic properties [11–13]. Defects are inherent in any system due to entropic reason. They (vacancy defect/impurity defect) can develop novel properties in 2D materials [14–18], and also electronic and magnetic properties of materials can be modified by defects [15, 19, 20]. People are using the pristine and defected G/MoS₂ HS in electronic devices. Hence, it is highly demanding to study HS of 2D materials with defects. The devices made by pristine G/MoS₂ HS and vacancy-defected G/MoS₂ HS sometimes have to be used in the surrounding (moisture) environment. Due to which, moisture (water molecule) can affect the properties of HS materials [21, 22]. The molecular adsorption in vacancy-defected HS can bring new properties because vacancy defects are very keen locations for molecular adsorption due

to the configuration of atoms around the vacancy. They play a particular role in determining the geometrical arrangement of layered materials [21–23]. Also, electronic and magnetic properties of defected materials can be modified by adsorbed water molecule [23]. Thus, it opens the way to tune novel properties of vacancy-defected HS materials. Therefore, it needs to study the adsorption of water molecule on G/MoS₂ HS (system-I) and Mo sites vacancy defects G/MoS₂ HS (system-II). To our best knowledge, literature studies do not contain a significant study of water-adsorbed 2D G/MoS₂ HS materials with Mo defects. In this study, we have investigated the structural, electronic, and magnetic properties of Mo sites vacancy-defected water-adsorbed 2D G/MoS₂ HS materials by using the spin-polarized density functional theory (DFT)-based first-principle calculations, within the DFT-D2 approach. Our calculations show that system-I and its Mo site vacancy defect (systems-II) materials could be promising candidates for the device applications.

The rest part of the article is arranged as follows. Computational methods, interpretation of findings, and conclusions of this study are given in Sections 2–4, respectively.

2. Methods and Materials

The comprehensive intuition is gained into the physical properties of the system-I and its Mo site vacancy defect systems-II by the spin-polarized density functional theory (DFT) [24]-based first-principle calculations. DFT with the PWscf code of the Quantum ESPRESSO package [25] has been conducted to study the structural, electronic, and magnetic properties of system-I and system-II. The code uses ultra-soft pseudo-potentials (USPPs) to describe the interactions between ion cores and valence electrons. A plane-wave basis set, with cut-off values of 35 Ry and 350 Ry for wave functions and charge densities, respectively, was used. Exchange and correlation interactions were considered by generalized gradient approximation (GGA) [26]. London dispersion contributions for weak vdW force in between the constituents of supercells were described through the DFT-D2 scheme [27]. Self-consistent field (Scf) and structure optimization calculations were executed by Broyden–Fletcher–Goldfarb–Shanno (BFGS) method [28] with Γ -centered Monkhorst-Pack (MP) [29] k -Points mesh commensurate with $(6 \times 6 \times 1)$ sampling of the heterostructures of system-I and system-II. The system-I was created by adsorbing water molecule (center position on the surface of MoS₂) at 2.52 Å distance above the top surface of MoS₂ in vertical G/MoS₂ HS as shown in Figure 1, since vertical G/MoS₂ HS was formed by (4×4) supercell structure of graphene and (3×3) supercell structure of MoS₂ with 4.11% lattice mismatch. In HS, the lattice mismatch can be determined via differing the lattice constant, whereas there is no direct chemical bonding between the component layers. Systems-II were constructed by adsorbing water molecule in centre-1Mo atom vacancy defect G/MoS₂ HS (system-IIa), left-1Mo atom vacancy defect G/MoS₂ HS (system-IIb), and 2Mo atom vacancy defect G/MoS₂ HS (system-IIc), which

are illustrated in Figure 2. Convergence was sustained by using Marzari–Vanderbilt (MV) [30] smearing with an enlightening of 0.001 Ry. David diagonalization methods with plain mixing mode for self-consistency where a default value of mixing factor 0.6 was used. To reduce the interaction within periodic structures, a vacuum detachment of 18 Å was used along z -direction. All the atoms in structures were allowed to relax by the PBE functional until the forces conversed to less than 10^{-3} Ry/Bohr in each direction and energy to 10^{-4} Ry. To tune electronic and magnetic properties of materials, a mesh of $(6 \times 6 \times 1)$ k -points was used for band structure calculations and meshes of $(12 \times 12 \times 1)$ k -points were employed for density of states (DOS) and projected density of state (PDOS) calculations.

3. Results and Discussion

In this section, we present, discuss, and analyze the main findings of this study. Findings of system-I and systems-II are obtained from band structure, DOS, and PDOS calculations.

3.1. Structural Study. The water-adsorbed G/MoS₂ HS is constructed by putting water molecule at various locations on graphene and MoS₂ surfaces of the G/MoS₂ HS material as shown in Figures 1(a)–1(d). The adsorbed water molecule (at center position on the surface of MoS₂) at a distance of 2.52 Å above the top surface of MoS₂ in the HS is found to be most stable, as shown in Figure 1(d). To determine the stability, we have calculated the binding energy of system-I by using the following equation [31]:

$$E_b = \frac{E_{w+G/MoS_2(HS)} - E_{G/MoS_2(HS)} - E_w}{A}, \quad (1)$$

where $E_{w+G/MoS_2(HS)}$, $E_{G/MoS_2(HS)}$, E_w are the total energy of the system-I, G/MoS₂ HS, and adsorbed water molecule, respectively, and “A” is the surface area of heterostructure. The obtained binding energy of system-I is $-23.82 \text{ meV}/\text{Å}^2$, which means system-I is energetically stable at the ground state. It means physisorption interaction takes place in between them. The stable optimized system-IIa, system-IIb, and system-IIc are created by adsorbing water molecule in centre-1Mo atom, left-1Mo atom, and 2Mo atom vacancy defect G/MoS₂ HS, respectively, as shown in Figures 2(a)–2(c). To determine the stability of such systems, we have also calculated binding energy using the following formalism [31]:

$$E_b = \frac{E_{w+G/MoS_2(HS)Mo-d} - E_{G/MoS_2(HS)Mo-d} - E_w}{A}, \quad (2)$$

where $E_{w+G/MoS_2(HS)Mo-d}$, $E_{G/MoS_2(HS)Mo-d}$, E_w are the ground state energy of Mo site vacancy defect water-adsorbed G/MoS₂ HS (systems-II), Mo site vacancy defect G/MoS₂ HS, and adsorbed water molecule, respectively, and “A” represents the surface area of defected heterostructures. The estimated binding energy of system-IIa, system-IIb, and system-IIc are $-20.09 \text{ meV}/\text{Å}^2$, $-20.03 \text{ meV}/\text{Å}^2$, and $-17.40 \text{ meV}/\text{Å}^2$, respectively. The calculated binding energy

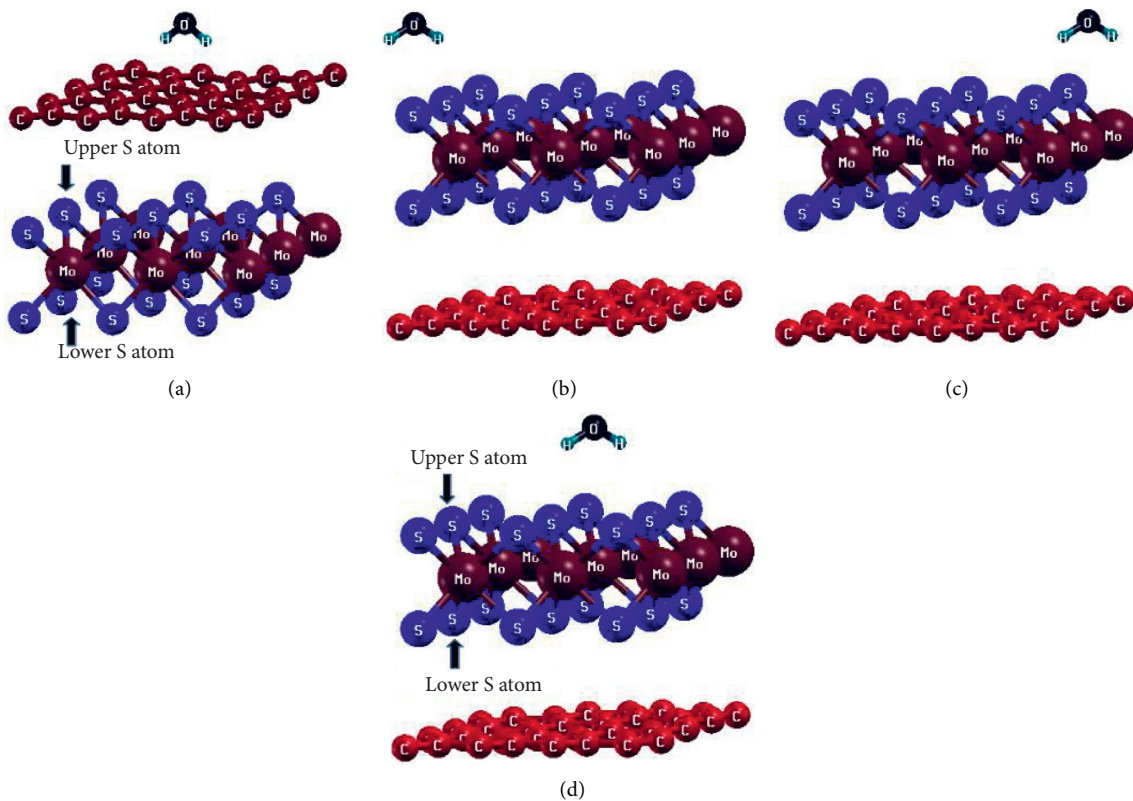


FIGURE 1: (a) Adsorbed water molecule is at 2.52 Å distance above the top surface of graphene in G/MoS₂ HS. (b) adsorbed water molecule is (left-position) at 2.52 Å distance above the top surface of MoS₂ in G/MoS₂ HS. (c) adsorbed water molecule is (right-position) at 2.52 Å distance above the top surface of MoS₂ in G/MoS₂ HS. (d) adsorbed water molecule is (center position) at 2.52 Å distance above the top surface of MoS₂ in G/MoS₂ HS.

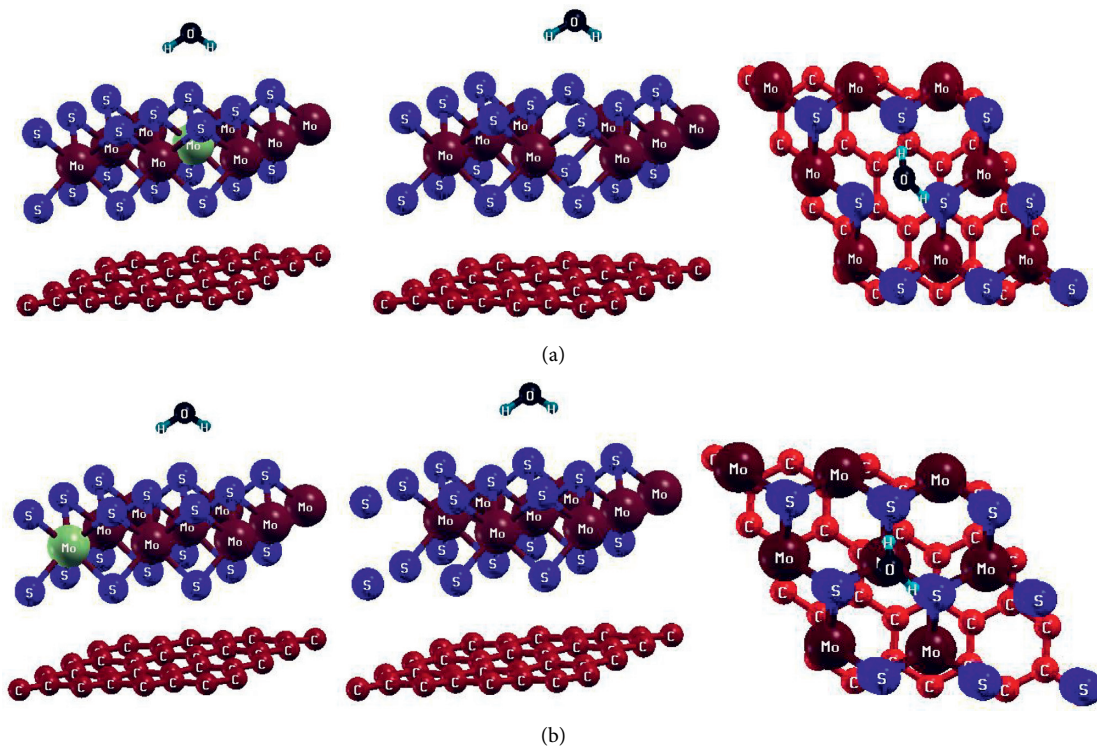


FIGURE 2: Continued.

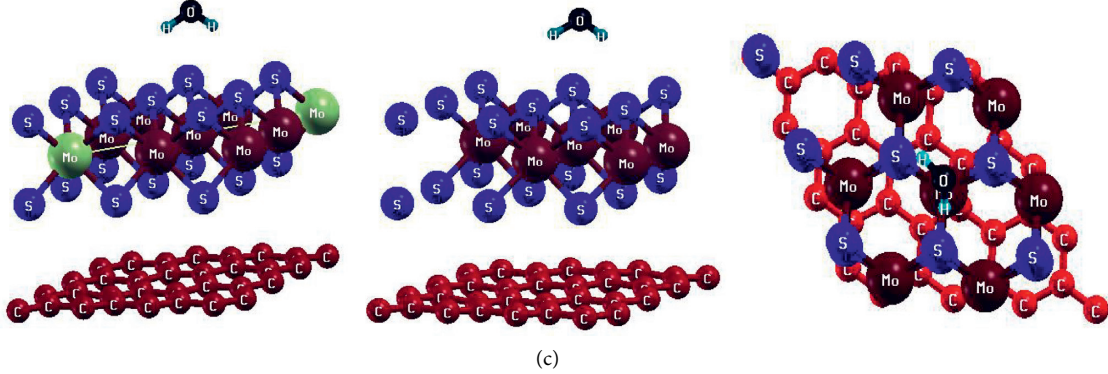


FIGURE 2: Side view and top view of Mo site vacancy defect HS materials: (a) center-1Mo atom vacancy defect water-adsorbed G/MoS₂ HS (system-IIa), (b) left-1Mo atom vacancy defect water-adsorbed G/MoS₂ HS (system-IIb), and (c) 2Mo atoms vacancy defects water-adsorbed G/MoS₂ HS (system-IIc).

of system-I, system-IIa, system-IIb, and system-IIc is comparable with the values of other vdW HSs [32, 33]. Thus, considered systems are stable because negative binding energy means that materials are energetically stable at the ground state. Lower value of binding energy indicates that the material is more stable than others. Hence, the stability of the above considered materials is decreased with an increase in the defect concentration. The defect formation energy of system-IIa, system-IIb, and system-IIc is found to be 0.21 eV, 0.21 eV, and 0.40 eV, respectively, which are calculated by using the following equation [34]:

$$E_{df} = (E_t)_d - [(E_t)_p + n_{Mo}\mu_{Mo}], \quad (3)$$

where $(E_t)_d$, $(E_t)_p$, n_{Mo} , and μ_{Mo} are the total ground state energy of vacancy defect HS (systems-II), total ground state energy of pristine HS (system-I), numbers of vacancy defects (Mo) atoms, and chemical potential of a Mo atom, respectively. Materials have lower defect formation energy, which indicates that they can be favorable for computational work.

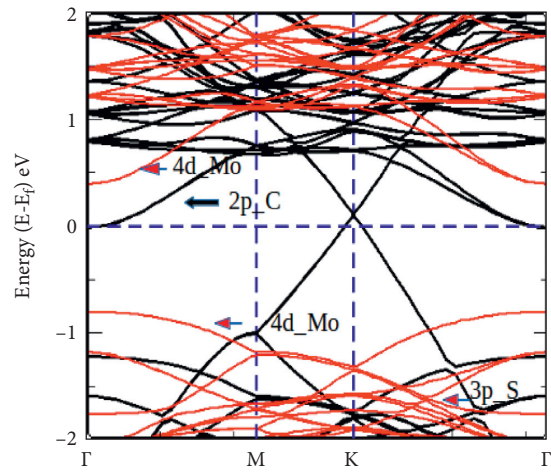
In addition, we have also computed the interlayers distance between graphene and monolayer MoS₂ of system-I, system-IIa, system-IIb, and system-IIc materials, and they are 3.72 Å, 3.81 Å, 3.83 Å, and 3.94 Å, respectively. These values are comparable with other graphene-based 2D HS materials [35, 36]. From this analysis, we conclude that system-I is more compact than Mo vacancy-defected systems. In systems-II, compactness of atoms and layers of constituents are increased with a decrease in their defect concentration. The estimation of binding energy and interlayer distance of the above considered systems shows that weak vdW force exists in between graphene and MoS₂.

3.2. Electronic Properties. The electronic properties of the material are predicted based on the electronic band structure. Band structures of system-I, system-IIa, system-IIb, and system-IIc are illustrated in Figures 3(a), 4(a), 5(a), and 6(a), respectively. We know that graphene and monolayer MoS₂ have metallic [1, 9] and semiconducting properties, respectively [12, 13]. Band structure of graphene/MoS₂ HS is a sum of band

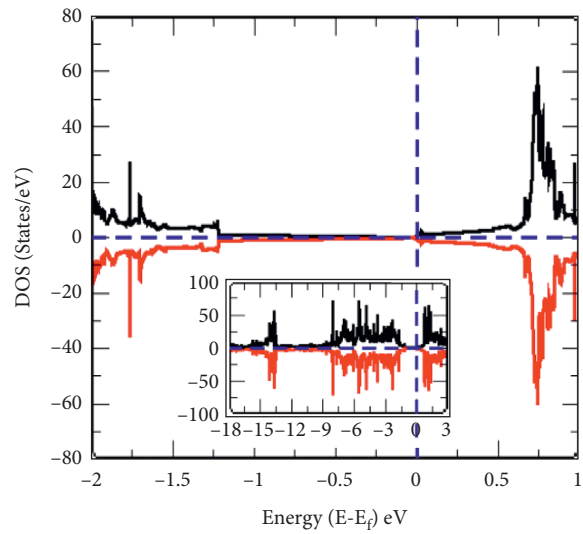
structures of those constituents in which properties of graphene are preserved, and hence, it also has metallic properties [20, 37]. Impressively, it is noted that Dirac point setup in the conduction band at 0.11 eV distance from the Fermi energy level in the band structure of water adsorbed Graphene/MoS₂ HS (system-I). This small value of the Dirac cone is obtained because of the adsorption of water molecule in G/MoS₂ HS. The formation of the Dirac cone in the conduction band means electrons spontaneously flow from the valence band to the conduction band. Hence, system-I has metallic properties. Also, the property of G/MoS₂ HS is still preserved.

Moreover, we explored band structures of systems-II materials and found that the Dirac cone is formed at 0.72 eV, 0.71 eV, and 0.68 eV distance from the Fermi energy level in system-IIa, system-IIb, and system-IIc materials, respectively, which are shown in Figures 4(a), 5(a) and 6(a). A few numbers of electronic bands of valence electrons cross the Fermi energy level in band structures, which is due to the effect of Mo vacancy atom in structures, which breaks the symmetry of system-I. Hence, defected materials are metallic. In systems-II, unpaired up-spin and down-spin states are appeared by Mo vacancy defects, due to which the movement of interfacial charges is developed in systems. Hence, the different values of the Dirac point, Fermi energy, and shift of the Fermi energy level towards the valence band are obtained in system-IIa, system-IIb, and system-IIc, which are presented in Table 1.

In Table 1, we can see that the values of Fermi energy and Fermi energy shift are increased with an increase in the concentration of Mo vacancy defects, but the distance of the Dirac point from the Fermi energy level decreases with an increase in the defect concentration in the systems. The reason is that vacancies are very precise place for adsorbed molecule. This is because we have calculated the bond length between nearest Mo-Mo atoms, S-S atoms, Mo-S atoms, and distance between adsorbed water molecule to MoS₂ surface in vacancy defects HS and found that the compactness of materials decreases with an increase in defect concentrations. Thus, adsorbed molecule disturbed the atomic configurations in vacancy-defected HS materials, which influences the electronic properties of the systems. Dirac



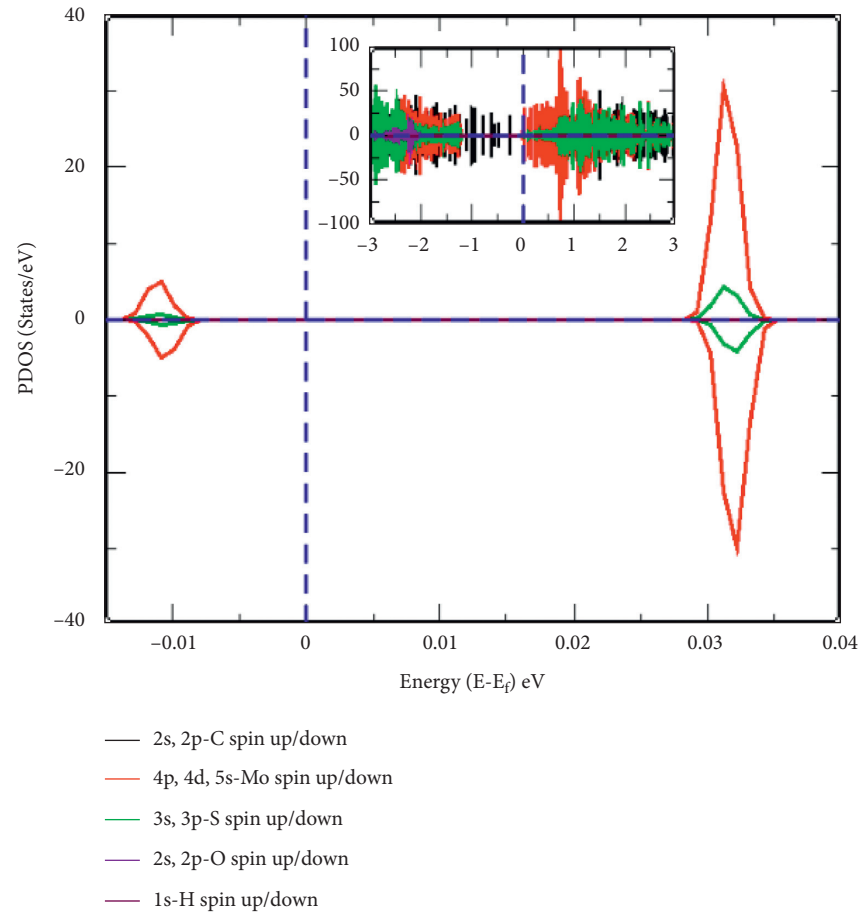
(a)



— spins up
— spins down

(b)

FIGURE 3: Continued.



(c)

FIGURE 3: Continued.

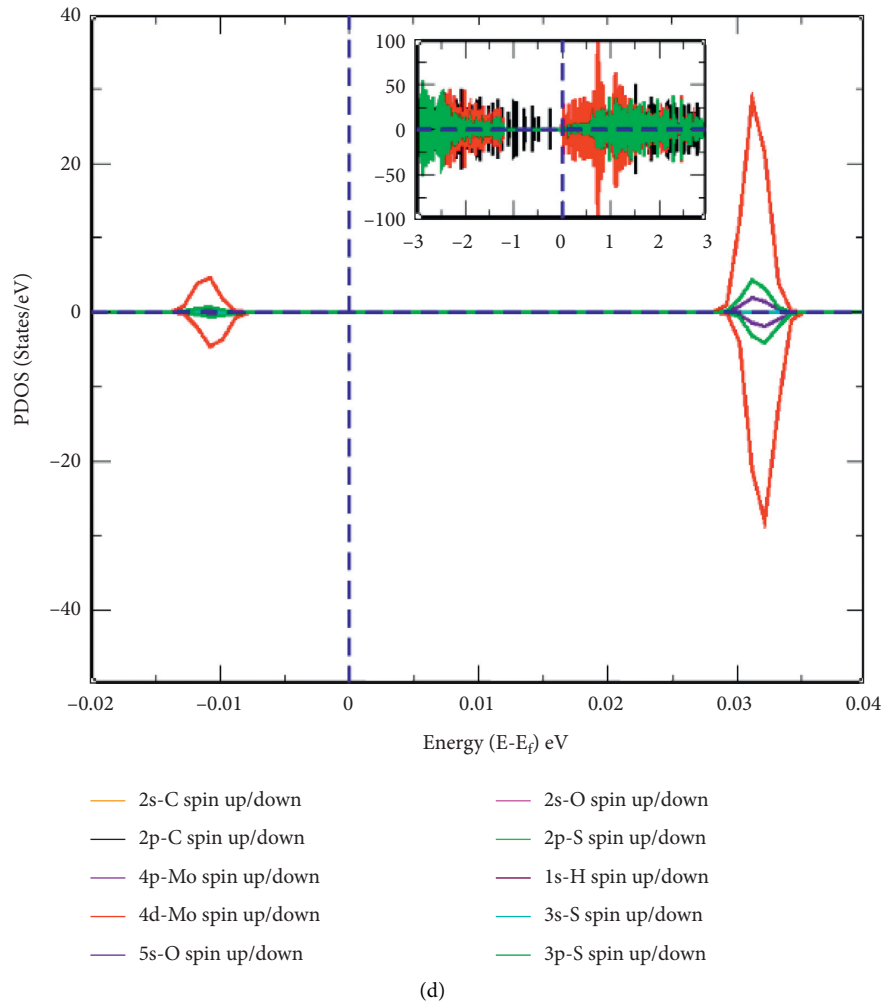


FIGURE 3: (a) Band structure of system-I, (b) DOS of up-spin and down-spin states of electrons in the orbitals of C Mo, S O, and H atoms of system-I, (c) PDOS of total up-spin and total down-spin states of electrons in the orbitals of C Mo, S O, and H atoms of system-I, (d) PDOS of individual up-spin and down-spin states of electrons in the orbitals of C Mo, S O, and H atoms of system-I. In all DOS and PDOS, the horizontal dot line separates spin states and the vertical dot line separates the electronic bands, and also in band plot, the horizontal dot line represents the Fermi energy level; insets in DOS and PDOS represent the spin states within a large energy range along x -axis.

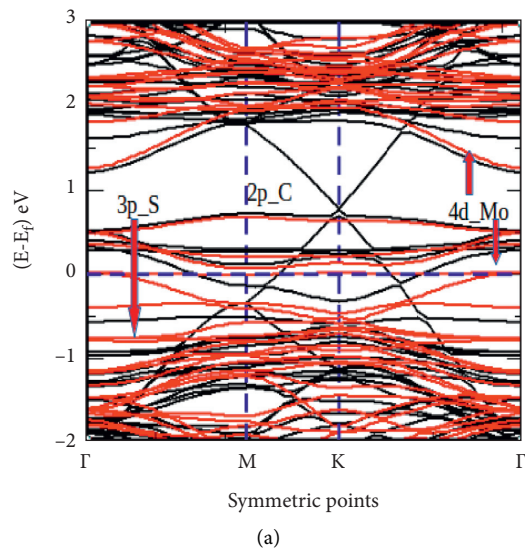


FIGURE 4: Continued.

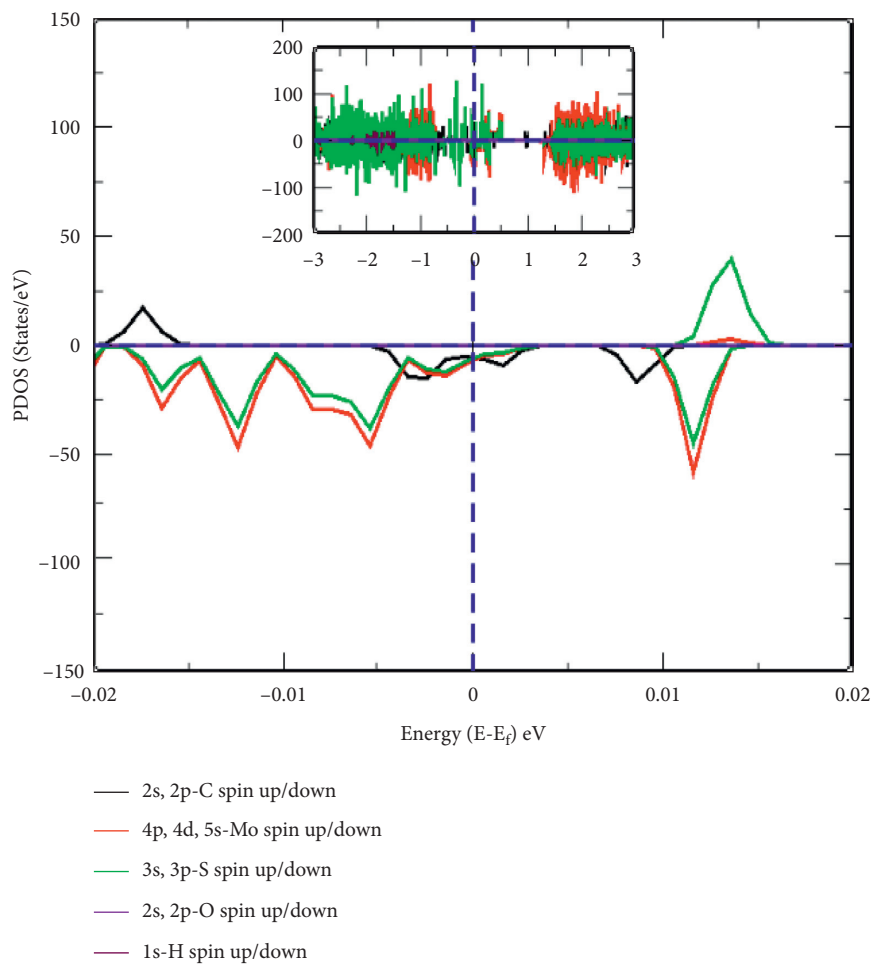
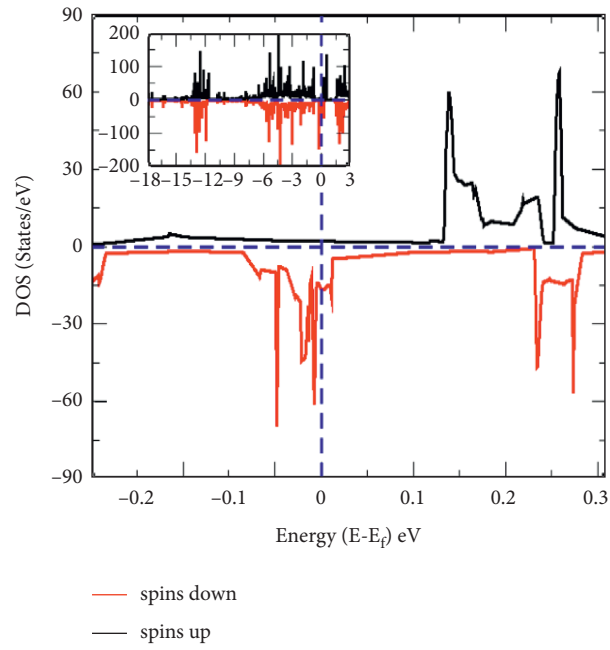


FIGURE 4: Continued.

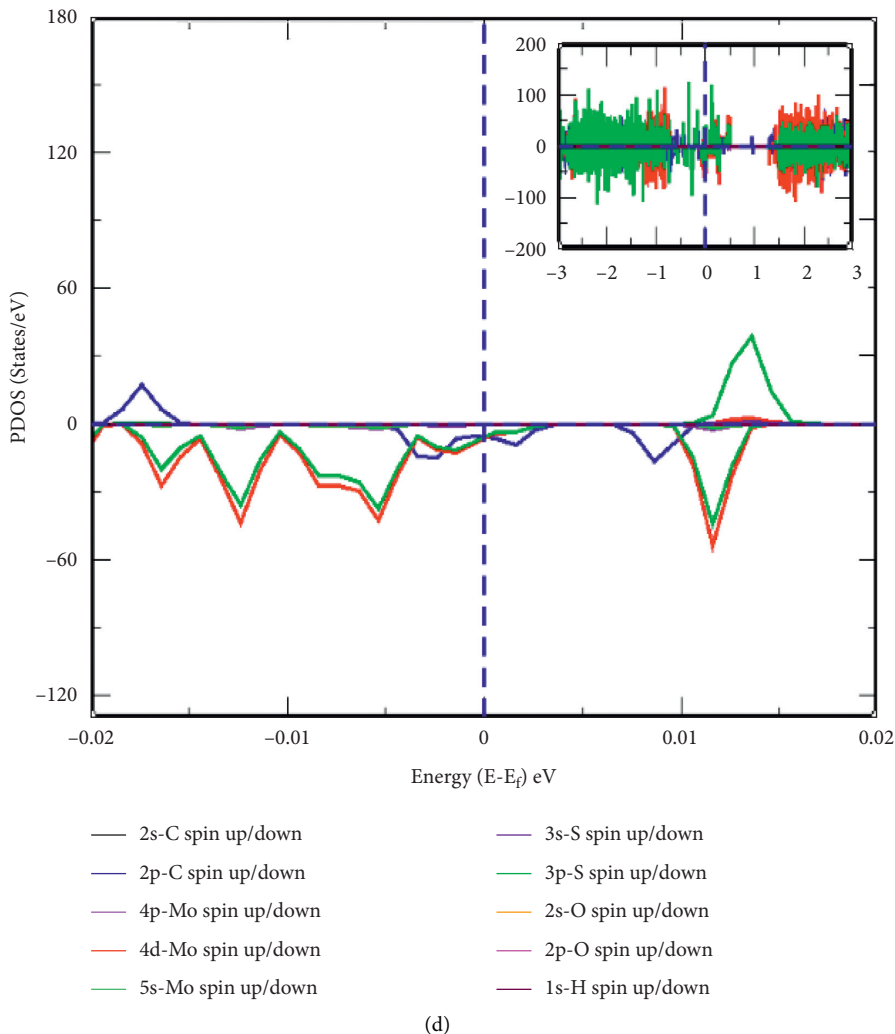


FIGURE 4: (a) Band structure of system-IIa, (b) DOS of up-spin and down-spin states of electrons in the orbitals of C Mo, S O, and H atoms of system-IIa, (c) PDOS of total up-spin and total down-spin states of electrons in the orbitals of C Mo, S O, and H atoms of system-IIa, (d) PDOS of individual up-spin and down-spin states of electrons in the orbitals of C Mo, S O, and H atoms of system-IIa. In all DOS and PDOS, the horizontal dot line separates spin states and the vertical dot line separates the electronic bands, and also in the band plot, the horizontal dot line represents the Fermi energy level. Insets in DOS and PDOS represent spin states within large energy range along x -axis.

point setup in the conduction band reflects that the electron impulsively proceeds from the valence to the conduction band because the flow of current in metals and semiconductors depends on the amplitude of Dirac shift. Hence, system-IIa, system-IIb, and system-IIc have metallic properties.

3.3. Magnetic Properties. The magnetic properties of materials can be studied based on the density of states (DOS) and the projected density of states (PDOS) analysis. DOS are defined as the number of available electronic states per unit energy range. In computational physics/chemistry, it is one of the ways to represent electronic eigen states in the energy space of a molecule, where it counts the number of energy states nearby a given energy value. If Ψ_i and E_i represent the normalized eigen functions and eigen

values, respectively, the total density of states (TDOS) can be defined as [17]

$$D(E) = \sum_i \delta(E - E_i), \quad (4)$$

where $D(E)$ represents the density of states, and its integral $\int D(E)dE$ in between the energies E_1 and E_2 gives the number of states within the specified energy range [38]. The density of states projected over any arbitrary state is defined as the projected density of states (PDOS). The present magnetic moment by reason of spin states of electrons in the individual orbital of atoms in the materials is calculated by using PDOS. It can be expressed as

$$n_0(E) = \sum_i |\langle f_0 | \Psi_i \rangle|^2 \delta(E - E_i), \quad (5)$$

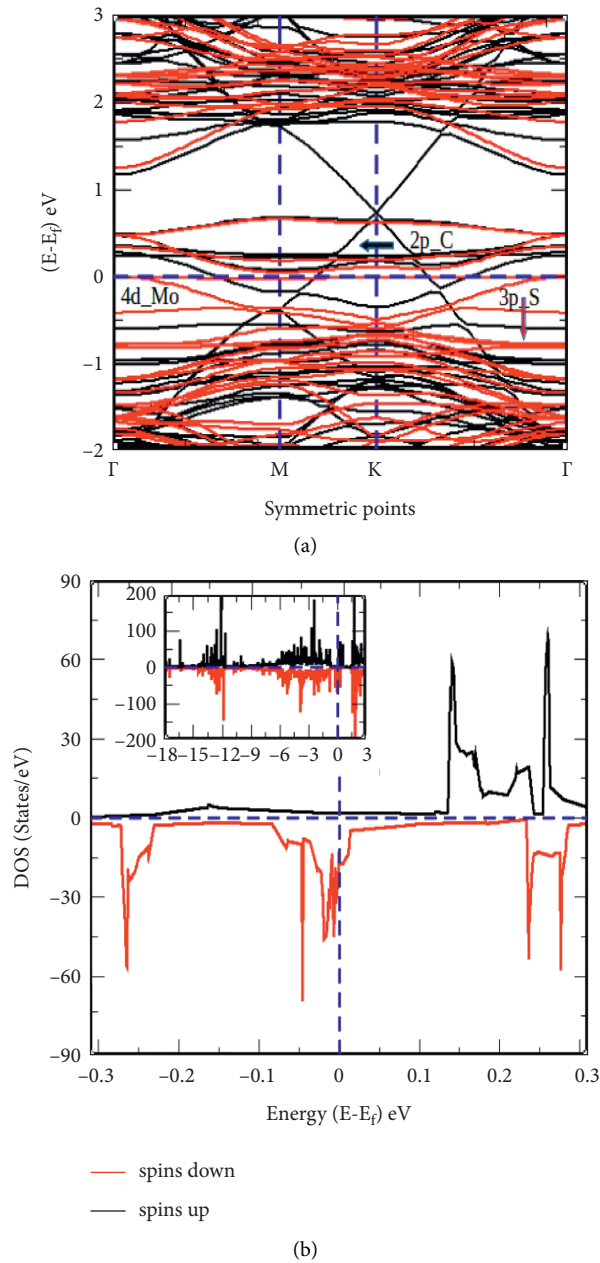
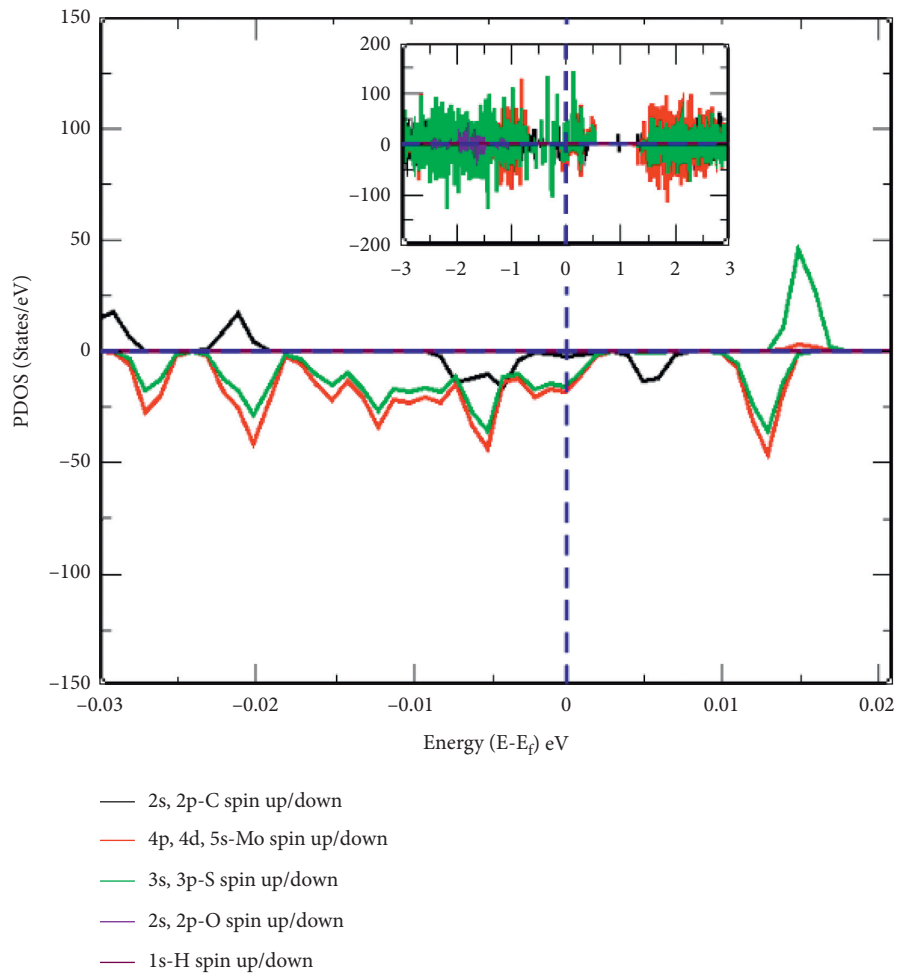


FIGURE 5: Continued.



(c)

FIGURE 5: Continued.

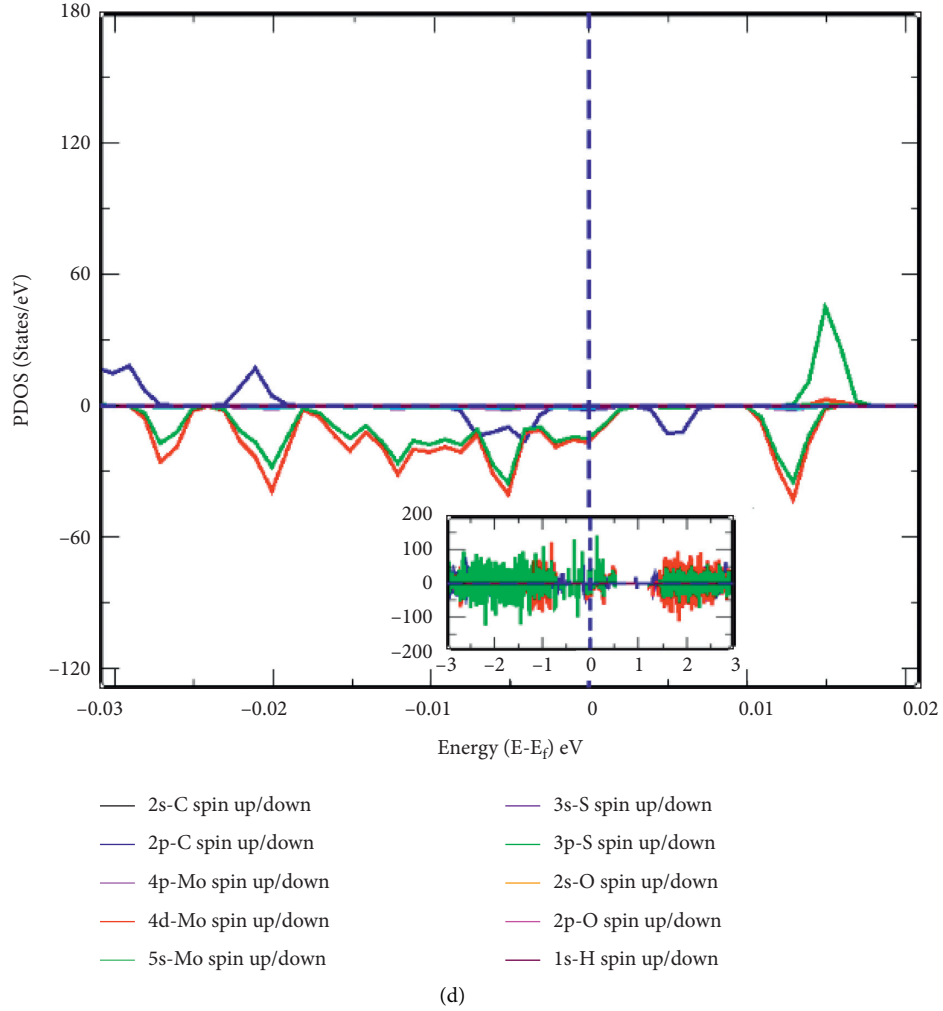


FIGURE 5: (a) Band structure of system-IIb, (b) DOS of up-spin and down-spin states of electrons in the orbitals of C Mo, S O, and H atoms of system-IIb, (c) PDOS of total up-spin and total down-spin states of electrons in the orbitals of C Mo, S O, and H atoms of system-IIb, (d) PDOS of individual up-spin and down-spin states of electrons in the orbitals of C Mo, S O, and H atoms of system-IIb. In all DOS and PDOS, the horizontal dot line separates spin states and the vertical dot line separates the electronic bands, and also in the band plot, the horizontal dot line represents Fermi energy level. Insets in DOS and PDOS represent the spin states within a large energy range along x -axis.

with $\int n_0(E)dE = 1$, due to the normalization condition of chosen orbital $|f_0\rangle$. When plotted, PDOS gives the relative contributions to TDOS and hence helps to analyze the relative contributions of each atom or molecule in the larger systems. Unpaired up-spin and down-spin states of an isolated atom possess a nonzero value of total spin and cause finite magnetic moment [19]. It means spin states are asymmetrically distributed in DOS and PDOS of materials. Up-spin and down-spin states are totally symmetric in DOS and PDOS, indicating equal contributions of magnetic moment in materials from up- and down-spin electrons. This ensures that those materials have nonmagnetic properties. In the present work, we discuss magnetic properties of water-adsorbed G/MoS₂ HS (system-I) and water-adsorbed Mo sites vacancy defect (systems-II) materials based on DOS and PDOS calculations. Magnetic moments due to spin states of C, Mo, S, O, and H atoms in PDOS of system-I and systems-II are given in Table 2.

DOS and PDOS plots for up-spin and down-spin electrons of system-I, system-IIa, system-IIb, and system-IIc are shown in Figures 3(b)–3(d), Figures 4(b)–4(d), Figures 5(b)–5(d), and Figures 6(b)–6(d), respectively. In Figures 3(b)–3(d), the DOS and PDOS plots for up-spin and down-spin of system-I are found to be symmetric, which means system-I is a nonmagnetic material. The system-IIa and system-IIb behave as strongly magnetic materials with largely asymmetric DOS/PDOS plots for up-spin and down-spin states near the Fermi energy level as shown in Figures 4(b)–4(d) and Figures 5(b)–5(d), while system-IIc is found to be slightly asymmetric as shown in Figures 6(b)–6(d), depicting the weak magnetic nature. We have calculated that the magnetic moment as asymmetrically distributed up-spin and down-spin states of electrons in 2s and 2p orbitals of C atoms are $0.00 \mu_B/\text{cell}$ & $0.03 \mu_B/\text{cell}$; 4p, 4d, and 5s orbitals of Mo atoms are $-0.03 \mu_B/\text{cell}$, $-0.75 \mu_B/\text{cell}$, and $-0.02 \mu_B/\text{cell}$;

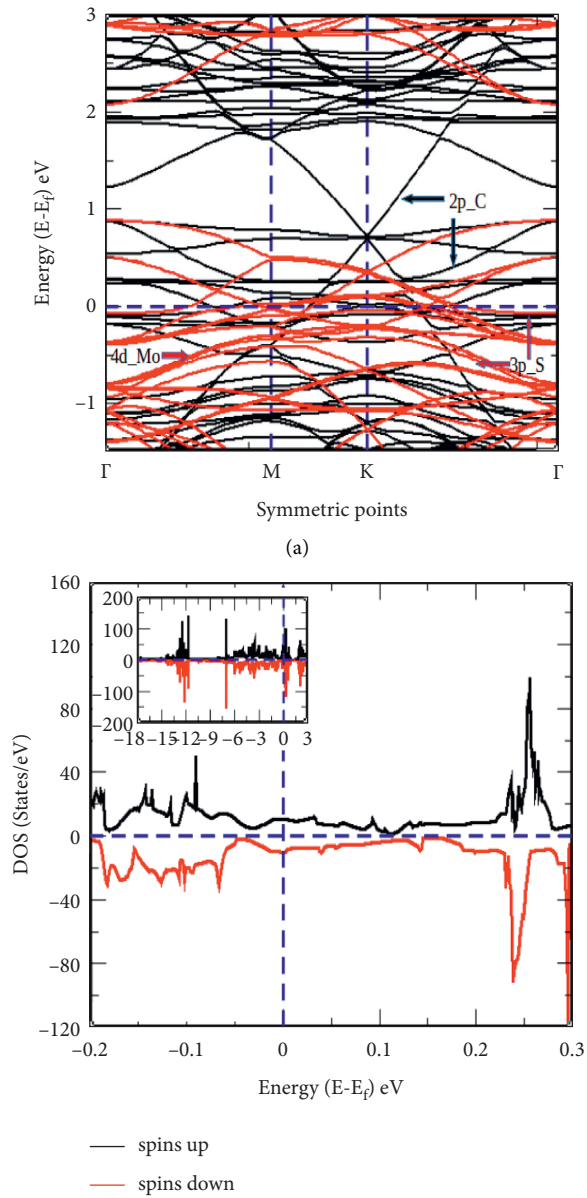
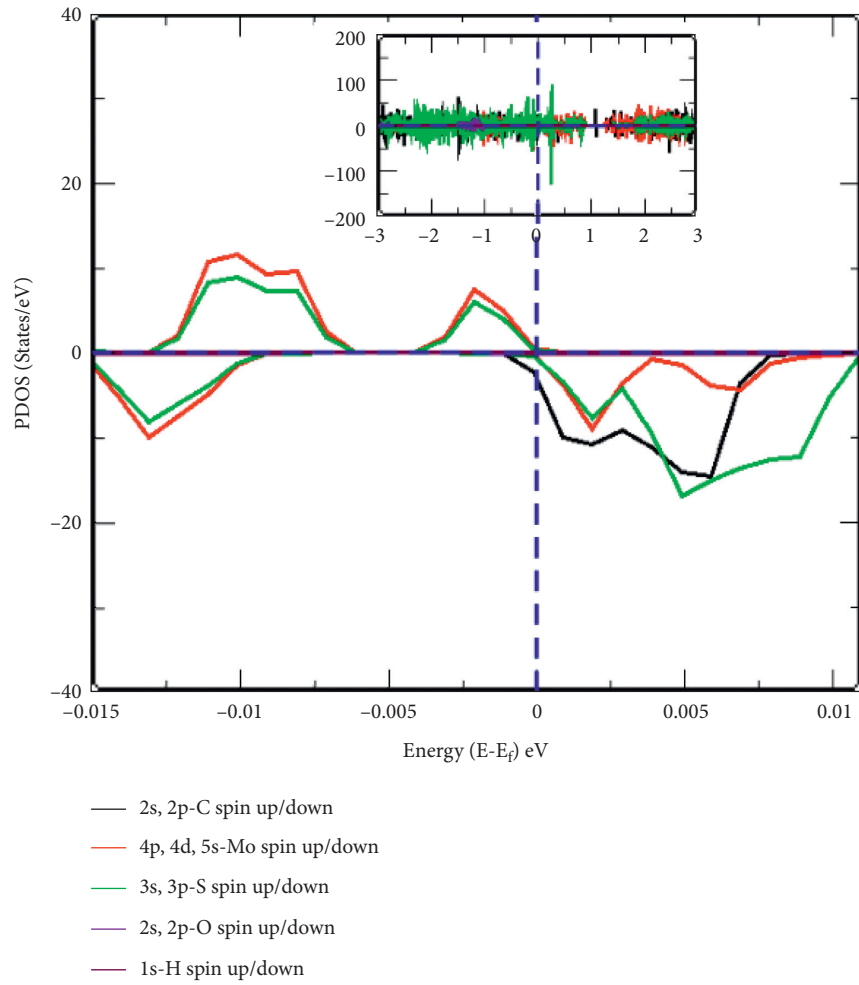


FIGURE 6: Continued.



(c)

FIGURE 6: Continued.

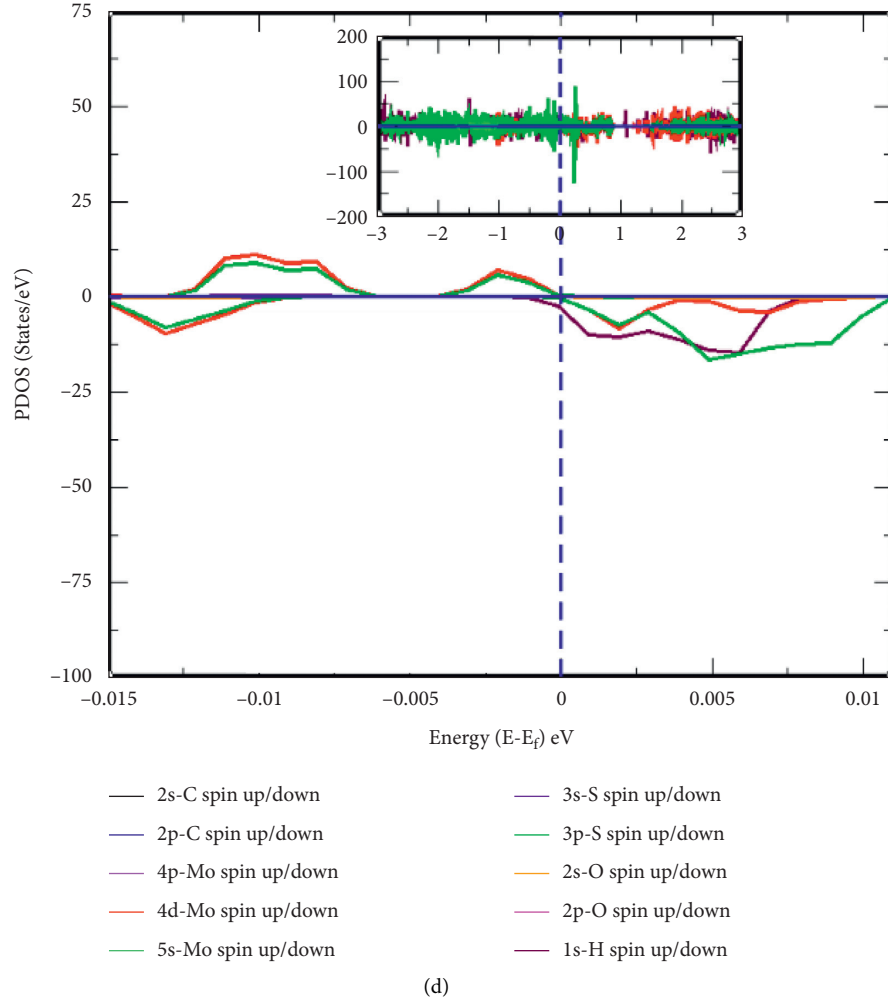


FIGURE 6: (a) Band structure of system-IIc, (b) DOS of up-spin and down-spin states of electrons in the orbitals of C Mo, S O, and H atoms of system-IIc, (c) PDOS of total up-spin and total down-spin states of electrons in the orbitals of C Mo, S O, and H atoms of system-IIc, and (d) PDOS of individual up-spin and down-spin states of electrons in the orbitals of C Mo, S O, and H atoms of system-IIc. In all DOS and PDOS, the horizontal dot line separates the spin states and the vertical dot line separates the electronic bands, and also in the band plot, the horizontal dot line represents the Fermi energy level. Insets in DOS and PDOS represent the spin states within a large energy range along x -axis.

TABLE 1: Fermi energy (E_f), fermi energy shifts (E_s), amplitude of the Dirac point (D_p), Dirac point shifts in defected materials (D_s), defect formation energy (E_{df}), and total binding energy of the systems (E_b).

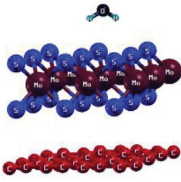
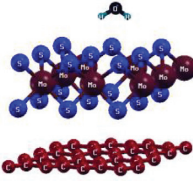
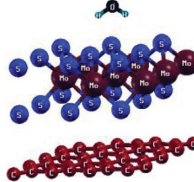
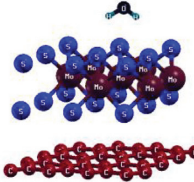
	System-I:	System-IIa:	System-IIb:	System-IIc:		
Systems \rightarrow						
Systems	E_f (eV)	E_s (eV)	D_p (eV)	D_s (eV)	E_{df} (eV)	E_b (meV/Å ²)
System-I	0.44	—	0.11	—	—	-23.82
System-IIa	-0.61	1.05	0.72	0.61	0.21	-20.09
System-IIb	-0.60	1.04	0.71	0.59	0.21	-20.03
System-IIc	-0.86	1.30	0.68	0.57	0.40	-17.40

TABLE 2: Total magnetic moment (μ_T) due to up-spin and down-spin state of electrons in the orbitals of C, Mo, S, O, and H atoms in PDOS of system-I, system-IIa, system-IIb, and system-IIc.

μ by up-spin and down-spin in \downarrow	System-IIc (μ_B/cell)	System-IIb (μ_B/cell)	System-IIa (μ_B/cell)	System-I (μ_B/cell)
2s of C	0.01	0.00	0.00	0.00
2p of C	0.02	0.03	0.03	0.00
4p of Mo	0.00	-0.02	-0.03	0.00
4d of Mo	0.04	-0.75	-0.75	0.00
5s of Mo	0.01	-0.02	-0.02	0.00
3s of S	0.02	-0.03	-0.04	0.00
3p of S	0.07	-1.72	-1.70	0.00
2s of O	0.00	0.00	0.00	0.00
2p of O	0.00	0.00	0.00	0.00
1s of H	0.00	0.00	0.00	0.00
μ_T (μ_B/cell)	+0.17	-2.51	-2.51	0.00

and 3s and 3p orbitals of S atoms are $-0.04 \mu_B/\text{cell}$ and $-1.70 \mu_B/\text{cell}$, respectively, of system-IIa. Thus, total magnetic moment of system-IIa has a value of $-2.51 \mu_B/\text{cell}$. Also, we have computed the magnetic moment by asymmetrically distributed unpaired up-spin and down-spin states of electrons in 2s and 2p orbitals of C atoms are $0.01 \mu_B/\text{cell}$ and $0.02 \mu_B/\text{cell}$; 4p, 4d, and 5s orbitals of Mo atoms are $-0.02 \mu_B/\text{cell}$, $-0.75 \mu_B/\text{cell}$, and $-0.02 \mu_B/\text{cell}$; 3s and 3p orbitals of S atoms are $-0.03 \mu_B/\text{cell}$ and $-1.72 \mu_B/\text{cell}$, respectively, in system-IIb. Hence, the total magnetic moment of system-IIb has a value of $-2.51 \mu_B/\text{cell}$. Similarly, we have determined the magnetic moment of system-IIc material due to asymmetrically distributed up-spin and down-spin states around the Fermi energy level in DoS/PDoS as shown in Figures 6(b)–6(d). The magnetic moments given by total up-spin and total down-spin states of electrons in the orbitals of C, Mo, and S atoms are found to be $0.03 \mu_B/\text{cell}$, $0.05 \mu_B/\text{cell}$, and $0.09 \mu_B/\text{cell}$, respectively. Also, we individually calculated the magnetic moments given by asymmetrically distributed spin states in 2s and 2p orbitals of C atoms, which have values of $0.01 \mu_B/\text{cell}$ and $0.02 \mu_B/\text{cell}$, respectively; 4p, 4d, and 5s orbitals of Mo atoms have values of $0.00 \mu_B/\text{cell}$, $0.04 \mu_B/\text{cell}$, and $0.01 \mu_B/\text{cell}$, respectively; and 3s and 3p orbitals of S atoms have values $0.02 \mu_B/\text{cell}$ and $0.07 \mu_B/\text{cell}$, respectively, as given in Table 2. Therefore, we found that the total value of magnetic moment of system-IIc is $+0.17 \mu_B/\text{cell}$. In summary, magnetic properties of materials are consistent with the spin-asymmetry theory for the origin of magnetism, where it is understood that the higher the net difference in electronic occupancy in between up-spin and down-spin, the higher the magnetic moment is. The calculated values of magnetic moment in system-IIa and system-IIb (i.e., $-2.51 \mu_B/\text{cell}$ and $-2.51 \mu_B/\text{cell}$) are greater than those of system-IIc ($+0.17 \mu_B/\text{cell}$) because unpaired spin states of electrons in the orbitals around the vacancy atoms of system-IIc seem to be more paired by absorbed water molecule than in system-IIa and system-IIb. Therefore, magnetic moment of system-IIc rapidly falls down compared to system-IIa and system-IIb. We also found that there is a bit stronger interaction of water molecule with 1Mo vacancy defects as compared to 2Mo vacancy defects in the systems; this is because of greater

polarizability of atoms in system-IIa and system-IIb than in system-IIc.

4. Conclusions

In this work, system-I, system-IIa, system-IIb, and system-IIc materials are constructed and investigated their structural, electronic, and magnetic properties by first-principles calculations based on the spin-polarized DFT-D2 method under computation package Quantum ESPRESSO. By analyzing the structures, we found that system-I is more compact than system-IIa, system-IIb, and system-IIc materials. Compactness of system and defect concentration in structures is related to each other because the more the defect concentrations in structures, the less the compactness of atoms in structures. Therefore, compactness of systems decreases with an increase in its defect concentration. On the analysis of band structures, system-I, system-IIa, system-IIb, and system-IIc have metallic properties. By studying DoS and PDoS calculations, we found that system-I has nonmagnetic properties and system-IIa, system-IIb, and system-IIc have magnetic properties. The total magnetic moment of system-IIa, system-IIb, and system-IIc has values $-2.51 \mu_B/\text{cell}$, $-2.51 \mu_B/\text{cell}$, and $+0.17 \mu_B/\text{cell}$, respectively. Higher values of magnetic moment are claimed by allotted up- and down-spins in 2p orbital of C atoms, 3p orbital of S atoms, and 4d orbital of Mo atoms in defected systems.

Data Availability

All the data to reproduce the figures and tables in the text can be obtained from the corresponding author.

Conflicts of Interest

The authors declare that they have no conflicts of interest.

Acknowledgments

The authors acknowledge the financial support from UGC Nepal grants Ph. D. 075/76-S & T-09, TWAS research grants RG 20-316, and network project NT-14 of ICTP/OEA.

References

- [1] K. S. Novoselov, A. K. Geim, S. V. Morozov et al., “Two-dimensional gas of massless dirac fermions in graphene,” *Nature*, vol. 438, no. 7065, pp. 197–200, 2005.
- [2] E. V. Castro, K. S. Novoselov, S. V. Morozov et al., “Biased bilayer graphene: semiconductor with a gap tunable by the electric field effect,” *Physical Review Letters*, vol. 99, no. 21, Article ID 216802, 2007.
- [3] L. Britnell, R. V. Gorbachev, R. Jalil et al., “Field-effect tunneling transistor based on vertical graphene heterostructures,” *Science*, vol. 335, no. 6071, pp. 947–950, 2012.
- [4] C. R. Dean, A. F. Young, I. Meric et al., “Boron nitride substrates for high-quality graphene electronics,” *Nature Nanotechnology*, vol. 5, no. 10, pp. 722–726, 2010.
- [5] X. Zhong, Y. K. Yap, R. Pandey, and S. P. Karna, “First-principles study of strain-induced modulation of energy gaps of graphene/BN and BN bilayers,” *Physical Review B*, vol. 83, no. 19, Article ID 193403, 2011.
- [6] L. Debbichi, O. Eriksson, and S. Lebegue, “Electronic structure of two-dimensional transition metal dichalcogenide bilayers from ab initio theory,” *Physical Review B*, vol. 89, no. 20, Article ID 205311, 2014.
- [7] F. Schedin, A. K. Geim, S. V. Morozov et al., “Detection of individual gas molecules adsorbed on graphene,” *Nature Materials*, vol. 6, no. 9, pp. 652–655, 2007.
- [8] S. J. Han, A. V. Garcia, S. Oida, K. A. Jenkins, and W. Haensch, “Graphene radio frequency receiver integrated circuit,” *Nature Communications*, vol. 5, no. 1, p. 3086, 2014.
- [9] T. Hu, A. Hashmi, and J. Hong, “Transparent half metallic $g\text{-C}_4\text{N}_3$ nanotubes: potential multifunctional applications for spintronics and optical devices,” *Scientific Reports*, vol. 4, no. 1, pp. 1–7, 2014.
- [10] S. Basu and P. Bhattacharyya, “Recent developments on graphene and graphene oxide based solid state gas sensors,” *Sensors and Actuators B: Chemical*, vol. 173, pp. 1–21, 2012.
- [11] L. Fornarini, F. Stirpe, B. Scrosati, and G. Razzini, “Electrochemical solar cells with layer-type semiconductor anodes: performance of $n\text{-MoS}_2$ cells,” *Solar Energy Materials*, vol. 5, no. 1, pp. 107–114, 1981.
- [12] Y. Zhang, J. Ye, Y. Matsushashi, and Y. Iwasa, “Ambipolar MoS_2 thin flake transistors,” *Nano Letters*, vol. 12, no. 3, pp. 1136–1140, 2012.
- [13] B. Radisavljevic, M. B. Whitwick, and A. Kis, “Small-signal amplifier based on single-layer MoS_2 ,” *Applied Physics Letters*, vol. 101, no. 4, Article ID 043103, 2012.
- [14] M. M. Ugeda, D. Fernández-Torre, I. Brihuega et al., “Point defects on graphene on metals,” *Physical Review Letters*, vol. 107, no. 11, Article ID 116803, 2011.
- [15] H. K. Neupane and N. P. Adhikari, “Structural, electronic and magnetic properties of impurities defected graphene/ MoS_2 van der waals heterostructure: first-principles study,” *Journal of Nepal Paediatric Society*, vol. 7, no. 2, pp. 1–8, 2021.
- [16] T. P. Kaloni, R. P. Joshi, N. P. Adhikari, and U. Schwingenschlög, “Band gap tuning in bn-doped graphene systems with high mobility,” 2014, <https://arxiv.org/abs/1402.0122>.
- [17] H. K. Neupane and N. P. Adhikari, “Effect of vacancy defects in 2D vdW graphene/h-BN heterostructure: first-principles study,” *AIP Advances*, vol. 11, no. 8, Article ID 085218, 2021.
- [18] H. K. Neupane and N. P. Adhikari, “Structural, electronic and magnetic properties of S sites vacancy defects graphene/ MoS_2 van der waals heterostructures: first-principles study,” *International Journal of Computational Materials Science and Engineering*, vol. 10, Article ID 2150009, 2021.
- [19] C. Kittel, *Introduction to Solid State Physics*, John Wiley & Sons, Hoboken, NJ, USA, 2005.
- [20] H. K. Neupane and N. P. Adhikari, “Structure, electronic and magnetic properties of 2D graphene-molybdenum disulphide (G-MoS_2) heterostructure (HS) with vacancy defects at Mo sites,” *Computational Condensed Matter*, vol. 24, Article ID e00489, 2020.
- [21] S. Lamichhane, P. Lage, G. B. Khatri, N. Pantha, N. P. Adhikari, and B. Sanyal, “First-principles study of adsorption of halogen molecules on graphene- MoS_2 bilayer hetero-system,” *Journal of Physics: Conference Series*, vol. 765, no. 1, Article ID 012011, 2016.
- [22] H. K. Neupane and N. P. Adhikari, “First-principles study of structure, electronic, and magnetic properties of C sites vacancy defects in water adsorbed graphene/ MoS_2 van der waals heterostructures,” *Journal of Molecular Modeling*, vol. 27, no. 3, pp. 1–12, 2021.
- [23] H. K. Neupane and N. P. Adhikari, “Structural, electronic and magnetic properties of defected water adsorbed single-layer MoS_2 ,” *Journal of Institute of Science and Technology*, vol. 26, no. 1, pp. 43–50, 2021.
- [24] P. Hohenberg and W. Kohn, “Inhomogeneous electron gas,” *Physical Review*, vol. 136, p. 864, 1964.
- [25] P. Giannozzi, S. Baroni, N. Bonini et al., “Quantum ESPRESSO: a modular and open-source software project for quantum simulations of materials,” *Journal of Physics: Condensed Matter*, vol. 21, no. 39, Article ID 395502, 2009.
- [26] J. P. Perdew, K. Burke, and M. Ernzerhof, “Generalized gradient approximation made simple,” *Physical Review Letters*, vol. 77, no. 18, pp. 3865–3868, 1996.
- [27] S. Grimme, “Accurate description of van der waals complexes by density functional theory including empirical corrections,” *Journal of Computational Chemistry*, vol. 25, no. 12, pp. 1463–1473, 2004.
- [28] B. G. Frommer, M. Côté, S. G. Louie, and M. L. Cohen, “Relaxation of crystals with the quasi-newton method,” *Journal of Computational Physics*, vol. 131, no. 1, pp. 233–240, 1997.
- [29] J. D. Pack and H. J. Monkhorst, “Special points for brillouin-zone integrations”—a reply,” *Physical Review B*, vol. 16, no. 4, pp. 1748–1749, 1977.
- [30] N. Marzari, D. Vanderbilt, A. De Vita, and M. C. Payne, “Thermal contraction and disordering of the Al(110) surface,” *Physical Review Letters*, vol. 82, no. 16, pp. 3296–3299, 1999.
- [31] T. V. Vu, N. V. Hieu, H. V. Phuc et al., “Graphene/ WSeTe van der waals heterostructure: controllable electronic properties and schottky barrier via interlayer coupling and electric field,” *Applied Surface Science*, vol. 507, Article ID 145036, 2020.
- [32] Q. Peng, Z. Guo, B. Sa, J. Zhou, and Z. Sun, “New gallium chalcogenides/arsenene van der waals heterostructures promising for photocatalytic water splitting,” *International Journal of Hydrogen Energy*, vol. 43, no. 33, pp. 15995–16004, 2018.
- [33] S. Li, M. Sun, J.-P. Chou, J. Wei, H. Xing, and A. Hu, “First-principles calculations of the electronic properties of SiC-based bilayer and trilayer heterostructures,” *Physical Chemistry Chemical Physics*, vol. 20, no. 38, pp. 24726–24734, 2018.
- [34] Z. Hou, X. Wang, T. Ikeda et al., “Interplay between nitrogen dopants and native point defects in graphene,” *Physical Review B*, vol. 85, no. 16, Article ID 165439, 2012.
- [35] S. Deng, L. Li, and P. Rees, “Graphene/ MoXY heterostructures adjusted by interlayer distance, external electric

- field, and strain for tunable devices,” *ACS Applied Nano Materials*, vol. 2, no. 6, pp. 3977–3988, 2019.
- [36] K. D. Pham, N. N. Hieu, H. V. Phuc et al., “First principles study of the electronic properties and schottky barrier in vertically stacked graphene on the janus MoSeS under electric field,” *Computational Materials Science*, vol. 153, pp. 438–444, 2018.
- [37] H. K. Neupane and N. P. Adhikari, “Tuning structural, electronic, and magnetic properties of C sites vacancy defects in graphene/MoS₂ van der waals heterostructure materials: a first-principles study,” *Advances In Condensed Matter Physics*, vol. 2020, Article ID 8850701, 11 pages, 2020.
- [38] G. Grosso and G. P. Parravicini, *Solid State Physics*, Academic Press, Cambridge, MA, USA, 2005.